Available online at www.sciencedirect.com
ScienceDirect
Journal of Power Sources 178 (2008) 603–609
JOURNAL OF POWER SOURCES
www.elsevier.com/locate/jpowsour

Pt–Co cathode electrocatalyst behaviour viewed by in situ XAFS fuel cell measurements

Agnieszka Witkowska [a,*], Sonia Dsoke [b], Emiliano Principi [c], Roberto Marassi [b], Andrea Di Cicco [c,1], Valerio Rossi Albertini [d]

[a] *Department of Solid State Physics, Gdansk University of Technology, 80-952 Gdansk, Poland*
[b] *Chemistry Department, University of Camerino, I-62032 Camerino (MC), Italy*
[c] *CNISM, CNR-INFM SOFT, Department of Physics, University of Camerino, I-62032 Camerino (MC), Italy*
[d] *ISM-CNR, via del Fosso del Cavaliere 100, 00133 Roma, Italy*

Received 12 July 2007; received in revised form 21 August 2007; accepted 22 August 2007
Available online 1 September 2007

Abstract

The paper presents a preliminary structural investigation of the 20% Pt–Co (1:1) alloy on Vulcan XC-72 catalyst using X-ray absorption spectroscopy (XAS), transmission electron microscopy (TEM) and X-ray diffraction (XRD). XAS results have been obtained ex situ and in situ using a specially optimized for XAS measurement fuel cell (down to 6 keV). The results are compared with those obtained for pure Pt catalyst on the same carbon support under the same working conditions.

Keywords: In situ X-ray absorption spectroscopy; Fuel cell; Pt–Co catalyst

1. Introduction

The cathode polarization is the main source of loss in low temperature polymer electrolyte membrane fuel cells (PEMFCs) and a lot of research activity is directed towards the development of catalysts with increased activity toward oxygen reduction reaction (ORR). Platinum alloys with transition metals, such as M = V, Cr, Co, Ti and Ni, as well as ternary alloys, exhibit significantly higher ORR electrocatalytic activities than Pt alone [1–4]. Although several hypotheses have been put forward in the literature to justify the reasons for this activity enhancements, the matter is still under debate. Many experimental works show that the increase in the kinetics of ORR compared to pure Pt could be attributed to changes in the geometric structure (i.e. Pt–Pt bond distance, number of Pt nearest neighbors, surface composition), in the electronic structure (i.e. orbitals energy levels, electron density of states in the Pt 5d band, strength of interaction between the Pt and M atoms) and to the nature and coverage of surface oxide layers [1,2,5–9]. Moreover, recent theoretical works suggest that sites like Pt–M or Pt–M–M are more active in promoting O_2 dissociation and that M atoms are better centers for OOH adsorption than Pt [10,11].

Several studies have been carried out to characterize the Pt–Co catalyst and to understand the chemical properties of the system [12–18], and references therein, but still some contradictory results may be found in the literature. For example, the stability of the alloy during operation, the mass activity enhancement factor in comparison to pure Pt and the influence of catalyst structure, ordering and atoms segregation on the catalytic reactivity are still under discussion.

In situ X-ray absorption spectroscopy (XAS) has been proved to be a powerful tool to investigate the fuel cell catalysts because of its ability to provide information regarding oxidation states and local coordination, numbers and identity of the neighbors of the absorbing atom. Several papers deal with the application of this technique in the fuel cell field [19]. Most of them have been performed ex situ or in situ with floated half cells [1,20–22]. Single cells equipped with fuel cell membrane electrode assembly (MEA) and without aqueous acidic electrolytes have

* Corresponding author. Present address: CNR-ISM Roma, Department of Physics, University of Camerino, I-62032 Camerino, Italy.
Tel.: +39 0737 40 25 50; fax: +39 0737 40 28 53.
E-mail address: agnieszka@mif.pg.gda.pl (A. Witkowska).
[1] Present address: IMPMC-CNRS, Universitè P.et M. Curie, 140 rue de Lourmel, 75015 Paris, France.

0378-7753/$ – see front matter © 2007 Elsevier B.V. All rights reserved.
doi:10.1016/j.jpowsour.2007.08.074

also been described in the literature by Viswanathan et al. [23], Roth et al. [24] and, more recently, by Wiltshire et al. [25]. The first two cells operate in transmission mode and, for this reason, require relative high loading of catalyst. The cell by Wiltshire et al. [25] operates in the fluorescence mode with lower requirements on catalyst loading. In our recent paper, we presented a single cell that can be operated in both transmission and fluorescence mode [26]. The high performance of this fuel cell, specially modified for in situ XAS measurements, permits to obtain X-ray absorption fine structure (XAFS) spectra in a large energy range (down to 6 keV) and for low metal loadings.

In this contribution, we report some of the XAS results obtained in situ using the above-mentioned fuel cell (XAS FC) in transmission mode at both Co K- and Pt L_3-edges for 20% Pt–Co (1:1) alloy on Vulcan XC-72 catalyst. The results are compared with those obtained for pure Pt catalyst on the same carbon support studied in the same working conditions.

2. Experimental

2.1. Samples preparation and XAS FC setup

Samples for ex situ and in situ measurements have been prepared as follows. Pellets for ex situ measurements were obtained by carefully mixing the 20% Pt–Co (1:1)/Vulcan XC-72 powder (E-TEK) and graphite powder (Alfa Aesar). The catalyst mass (metal thickness) was chosen to give optimal jump at the selected absorption edges, i.e. 0.4 for Co K-edge and 0.7 for Pt L_3-edge. The pellet, 13 mm in diameter and 0.5–1 mm thick, was mounted in a vacuum chamber and XAS spectra were collected at room temperature. For in situ measurements, membrane electrode assemblies (MEAs) were prepared. The MEA, with an active area of 5 cm^2, consisted of two electrodes with catalytic layers formed on the commercially available gas diffusion media (ELAT GDL (LT1200W) from E-TEK) and Nafion NRE-212® (thickness 50 μm) the proton conductive membrane. The catalytic layers were prepared using E-TEK products: 30% Pd/Vulcan XC-72 powder for the anode (with total Pd loading of 1.0 mg cm^{-2}) and 20% Pt–Co (1:1)/Vulcan XC-72 powder for the cathode (with Pt loading of 0.64 mg cm^{-2} and Co loading of 0.19 mg cm^{-2}). Palladium was used as anode catalyst as the energy of the core levels is outside the X-ray energy range of interest. For the preparation of the inks the required quantity of metal/Vulcan catalytic powders were placed in a closed glass vial with isopropyl alcohol and 5% Nafion solution (Nafion content was 35 wt.%). The suspension, stirred at room temperature for 24 h, was then brushed on the GDL and dried at 80 °C for 30 min. The metal loading was computed from the weight. The Nafion membrane was sandwiched between the two electrodes in the specially optimized for in situ XAS measurements fuel cell (XAS FC) without hot pressing. The cell is described in detail in [26]. Briefly, a commercial cell has been modified by thinning the graphite plates, down to 0.25 mm in thickness, behind the flow channels. The truncated prism-shaped holes, flat area 1 mm ×7 mm, provide a double window for XAS in transmission and fluorescence modes. The tests indicate that useful spectra can be collected over the large energy range, starting from 6 keV (with transmissions of around 10%). In other words, using this fuel cell prototype, XAS measurements can be performed in transmission and fluorescence modes for a wide selection of catalyst materials (atomic numbers above $Z = 23$).

Cell graphite plates were held together by eight screws, inducing high enough compression of the MEA to ensure good electrical contact and gas tightness. The cell was operated connecting its inlets to an oxygen and hydrogen supply. Hydrogen and oxygen flows were optimized to about 100 ml min^{-1} and the gasses were pre-humidified using bubblers. All the measurements were performed at room temperature and atmospheric pressure. The cell was polarized galvanostatically or potentiostatically using an AMEL 7050 galvanostat–potentiostat driven by a LabView-based computer program. Current and potential were measured continuously during XAS data acquisition and stored with the structural data.

Normally before collecting any XAS spectra, the cell was preconditioned at room temperature and at voltage about 0.5 V for several hours and its electrochemical performance was checked. A typical polarization curve obtained with the described experimental setup is shown in Fig. 1. XAS spectra were collected while holding the potential at selected values (see arrows in Fig. 1).

2.2. XAS measurements and EXAFS analysis

The spectra at the Co K-edge and Pt L_3-edge of Pt–Co nanoparticles and Co and Pt foils were recorded at the Synchrotron Light Laboratory ELETTRA (XAFS Station, Trieste, Italy) using a double-crystal monochromator equipped with Si(1 1 1) crystal. Measurements were performed at room tem-

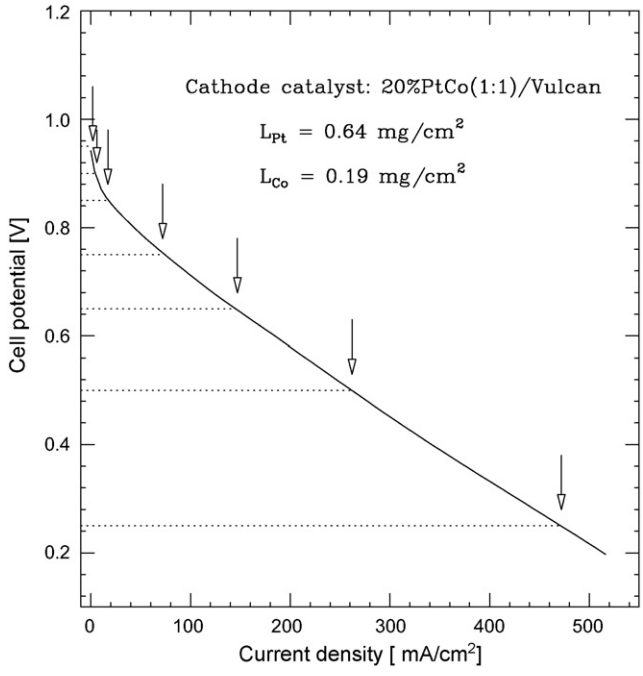

Fig. 1. Room temperature polarization curve obtained using in situ XAS FC setup for 20% Pt–Co (1:1)/Vulcan cathode electrocatalyst. Arrows indicate the points at which XAFS measurements were performed.

perature ex situ and in situ. Data were collected over the whole XAFS range: 11.4–12.8 keV for Pt (Pt L_3-edge energy is 11.564 keV), and 7.5–8.3 keV for Co (Co K-edge energy is 7.7 keV).

To obtain acceptable quality spectra, each XAFS measurement was repeated twice and averaged for successive processing (integration time was 2 s per point, total acquisition time equaled to about 60 min). The sampling procedure was chosen to yield data available for both pre- and post-edge background analyses used to normalize the spectra.

The experimental EXAFS data have been object of a preliminary analysis with an advanced technique using theoretical calculations of the X-ray absorption cross-section in the framework of the GNXAS method [32,33]. GNXAS method allows for a proper inclusion of "ab initio" multiple scattering (MS) contributions in the EXAFS data-analysis. Details of the methodology applied to the EXAFS data-analysis obtained for nanostructured materials are described in [27].

In the case of the Pt–Co alloy catalyst, a simultaneous two-edge analysis (Co K and Pt L_3) have been performed. Using this approach, the closer-shell distributions are determined accurately, because the parameters defining these distributions are related to the direct two-body signals and several MS contributions calculated for both Co K- and Pt L_3-edges. The background models for Co K and Pt L_3signals were the same used in the bulk crystallines (Co and Pt foils, respectively). The other nonstructural parameters (S_0^2, E_0) were fixed to the values obtained for bulk materials within their estimated uncertainty.

2.3. TEM and XRD measurements

Transmission electron microscopy (TEM) images have been taken using a Philips CM-10. Particles size distribution, on the base of the profile of 200 randomly selected quasi-spherically shaped particles, has been obtained using ImageJ program (image processing and analysis program).

X-ray powder diffraction patterns were obtained by a Philips diffractometer (PW1830 X-ray generator) with Bragg-Brentano geometry. Cu K α radiation (λ = 1.5406 Å) was monochromatised by means of a graphite crystal. Step-scan patterns were collected in the 30° to 90° 2θ range, with 0.02° step and 4 s per point counting time.

3. Results

3.1. Pt–Co alloy structure characterization

The activity of nanocatalyst strongly depends on the particles size, shape and structural details at the atomic level, related to bond distance, ordering and surface composition. For this reason, accurate morphological investigations and structural characterization should be performed prior to any effort to correlate XANES data with electrochemical behaviour. Besides, it is known that Pt–Co alloy can crystallise in both face-centered cubic (fcc) and tetragonal phases (depending on the alloy composition), in ordered and substitutionally disordered form [28].

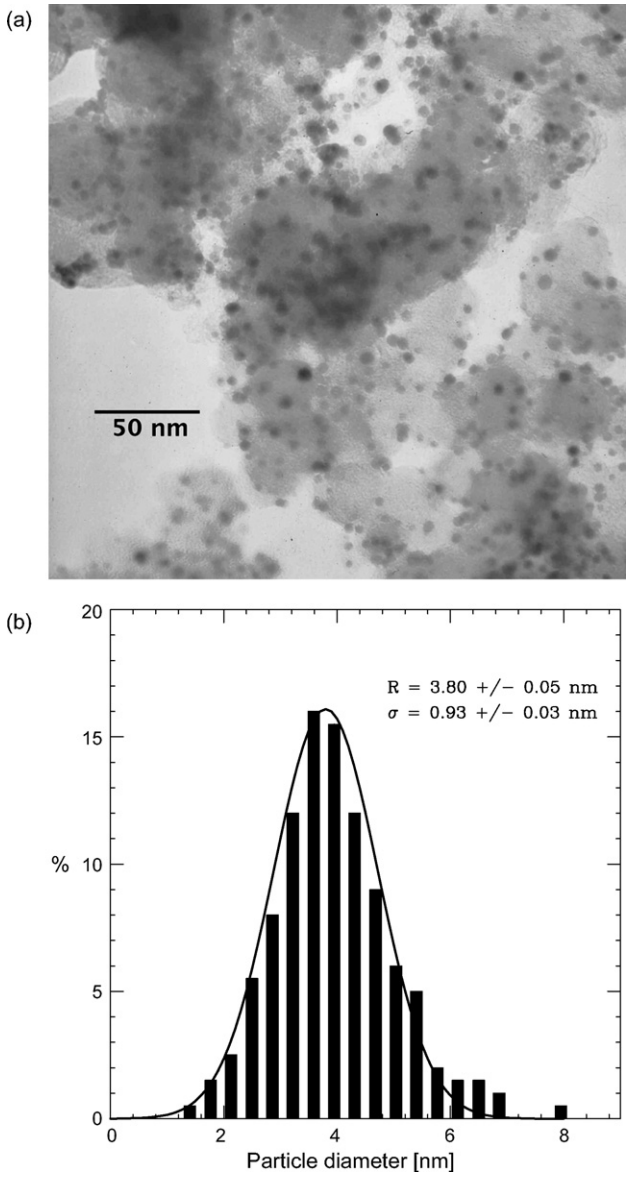

Fig. 2. Typical TEM image of the Pt–Co catalytic material (a) and obtained nanoparticle size distribution (b).

Additionally, in some nanostructured Pt–Co alloys, a segregation of one type of atoms on the surface of nano-grains has been observed [13,14] or corrosion of cobalt, forming pure or almost pure platinum "skin", has been noted [7,29]. Therefore, we have used transmission electron microscopy (TEM) and X-ray diffraction (XRD) measurements to obtain various essential information about the samples.

TEM-image analysis has been performed to study the actual nanoparticle size distribution. Fig. 2a shows a typical TEM image of Pt–Co nanoparticles with nearly spherical shape and Fig. 2b presents the obtained size distribution. It should be noted that the distribution is asymmetric and shows a tail extended to large-sized nanoparticles. However, the size distribution can be reproduced rather accurately through a Gaussian model. The mean particle diameter is found to be 3.80 ± 0.05 nm with standard deviation 0.93 ± 0.03 nm, consistently with product data-sheet information from E-TEK.

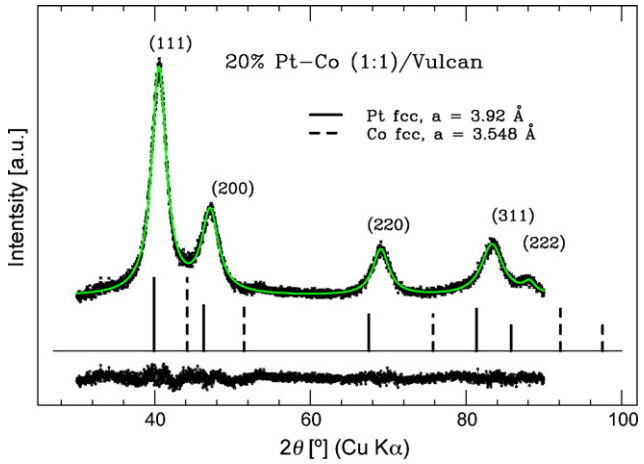

Fig. 3. X-ray powder diffraction pattern of the Pt–Co nanocatalyst. Experimental data (points) are compared with the calculations using Voigt functions (solid line). The agreement with calculated spectrum is very good, and the residual curve is shown below the diffraction pattern. Solid and dashed vertical lines show calculated peak positions for Pt fcc and Co fcc structures, respectively (lattice parameter taken from [31]).

Fig. 3 shows a typical X-ray diffraction pattern from which, through Scherrer equation [30], the mean Pt–Co crystallite size can also be estimated. The broadening of the peaks observed in the pattern directly indicates that the catalyst is a nanostructured material with small grain size. The line profiles of the peaks (1 1 1), (2 0 0), (2 2 0), (3 1 1) and (2 2 2) have been modeled with a Voigt function, using a Gaussian component to correct for instrument contribution to peak broadening. Taking into account that the particle size distribution is relatively narrow (Scherrer constant $K = 0.9$), the average size of Pt–Co nanoparticles, as obtained by averaging the results of the data-analysis of the 5 Bragg peaks, resulted to be 3.5 ± 0.4 nm, in fair agreement with TEM result.

No additional peaks or shoulders are observed in the X-ray diffraction patterns. This indicate that the nanoparticles are a Pt–Co alloy. The crystalline structure is consistent with a fcc phase with lattice parameter $a = 3.843$ Å (contraction of about 2% compared to unit cell lattice parameter of 20% Pt/Vulcan catalyst [27]). Moreover, the angular positions of the peaks, very close to the expected fcc pure Pt values, suggest a possible presence of a Pt-rich alloy.

3.2. XANES analysis

Comparison of the normalized spectra in the XANES range of Pt–Co alloy electrocatalyst at different potentials, as indicated in the polarization curve in Fig. 1, shows changes in the shape and intensity of features observed near the edge region for both Co K- and Pt L_3-edges (Fig. 4a and b, respectively). Generally, the differences in the XANES region are mainly related to change in the electronic properties. This is expected in the case of alloy formation. In fact, during alloying, charge transfer from cobalt to platinum occurs and the cobalt population levels involved in transitions 1s →4s/4p and 1s → 3d rearrange [34,35].

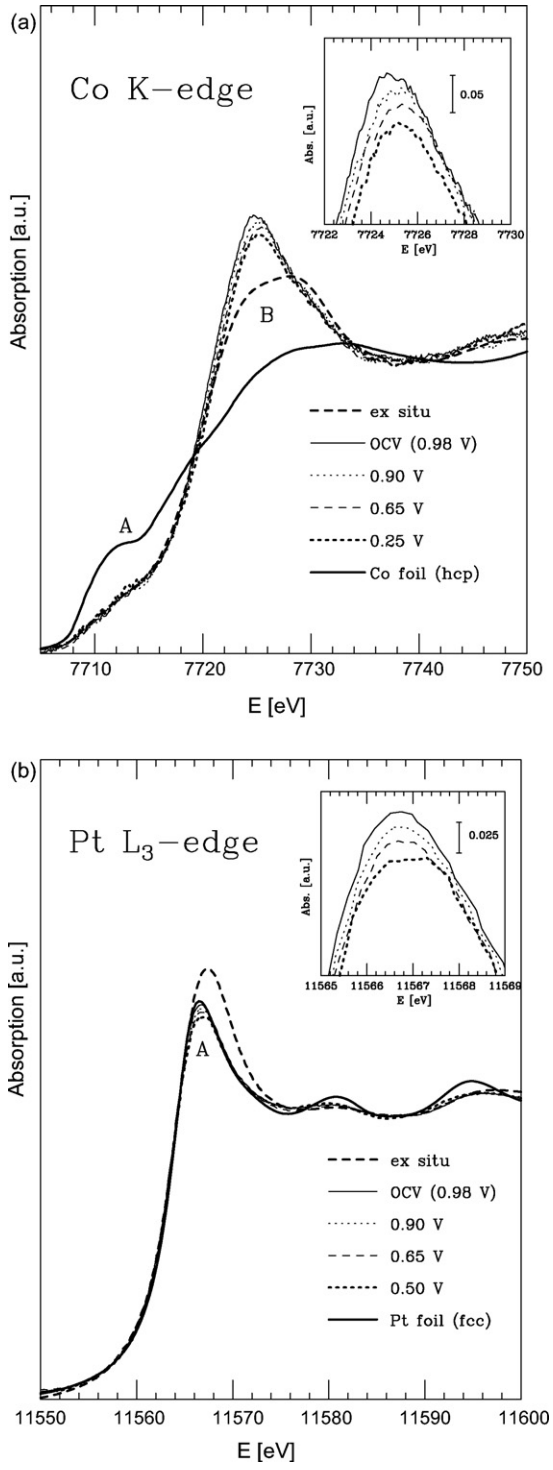

Fig. 4. Normalized XANES spectra (after background substraction) of 20% Pt–Co (1:1)/Vulcan cathode electrocatalyst collected in situ at RT and under various working conditions at: (a) Co K-edge and (b) Pt L_3-edge.

The changes in features A and B for Co K-edge (see Fig. 4a) describe mainly 3d and hybridized 4s, 4p bands occupancy, respectively [34]. The variation of the feature B of Co K-edge could also depend on multiple scattering effects, correlated with clearly observable structural changes in the Co neighborhood (compare the spectra of Co hcp foil and Pt–Co fcc disordered

alloy measured ex situ in Fig. 4a). The integrated intensity of the Pt L_3white line (WL, peak A in Fig. 4b) gives information about 5d-electron vacancy [19], which results in an increase of the WL with increasing of the vacancy (decrease of 5d-electron density).

No change in feature A and increase of peak B intensity, compared to ex situ spectra, occur, as shown in Fig. 4a for working MEA at Co K-edge. These effects could be related to oxidation of surface cobalt atoms upon the fuel exposure. Subsequently, during operation decreasing potential value induces a progressive Co reduction (see inset in Fig. 4a).

For Pt L_3 XANES measurements, see Fig. 4b, all the spectra are rather similar to that of Pt foil, indicating that platinum atoms in the nanoparticles are in the metallic state and keep fcc structure. The Pt L_3WL magnitude of Pt–Co working catalyst decreases with respect to the ex situ measurement and becomes comparable with that of Pt foil. This means that, upon exposure of the cathode catalyst to the fuel, the Pt atoms from nanoparticles surface are strongly reduced. Further variations of electrochemical conditions induce slight changes only. Close examination of Fig. 4b (see also the inset) shows that the decrease in the WL intensity is correlated with the decrease of electrode potential (the same tendency as in the Co K-edge). It should be also noted that, in the Pt L_3 XANES range, potential-dependence is not so pronounced as in the case of Co K (compare insets of Fig. 4a and b).

In addition, for Pt–Co alloy, the WL intensity measured in situ conditions is lower than that collected for pure platinum, i.e. 20% Pt/Vulcan cathode electrocatalyst (with the same metal loading, the same support and at the same working conditions) as shown in Fig. 5. Regardless the working potential, nanostructure Pt is more metallic when it is alloyed with Co than when it is in its pure form, and also its electronic structure is more stable. This phenomenon can be explained by a strong electronic interaction between Pt and Co atoms, which leads up to pronounced decreasing in Pt strength on the adsorption of oxygenated species. As a consequence, electroreduction activity of Pt in presence of this transition metal increases [2–4], and references therein.

3.3. EXAFS analysis

To gain further structural information on the atomic level two-edge EXAFS analysis have been performed and some preliminary results are presented in Fig. 6a and b for the Co K- and Pt L_3-edges, respectively. The results could be summarized as follows:

- the Pt–Co alloy is evidently a nanostructured alloy with basal fcc phase, in agreement with the XRD result. This could be clearly observed from the decrease of FT peaks intensity (indicating the nanometric nature of the catalyst) and from the shape and positions of the FT peaks, well correlated with the fcc structure;
- the Co local structure is very disordered (probably due to high substitutional disorder and/or presence of amorphous Co phase) as evidenced by the significant decrease of the intensity of FT peaks in Fig. 6a and also from high disorder structural parameters;
- the Pt local structure is ordered, as results from the values of the parameters describing Pt–Pt distribution: $\sigma^2 \approx 0.005$ Å^2 and $\beta \approx 0.2$ (Debye–Waller and distribution asymmetry parameters, respectively);

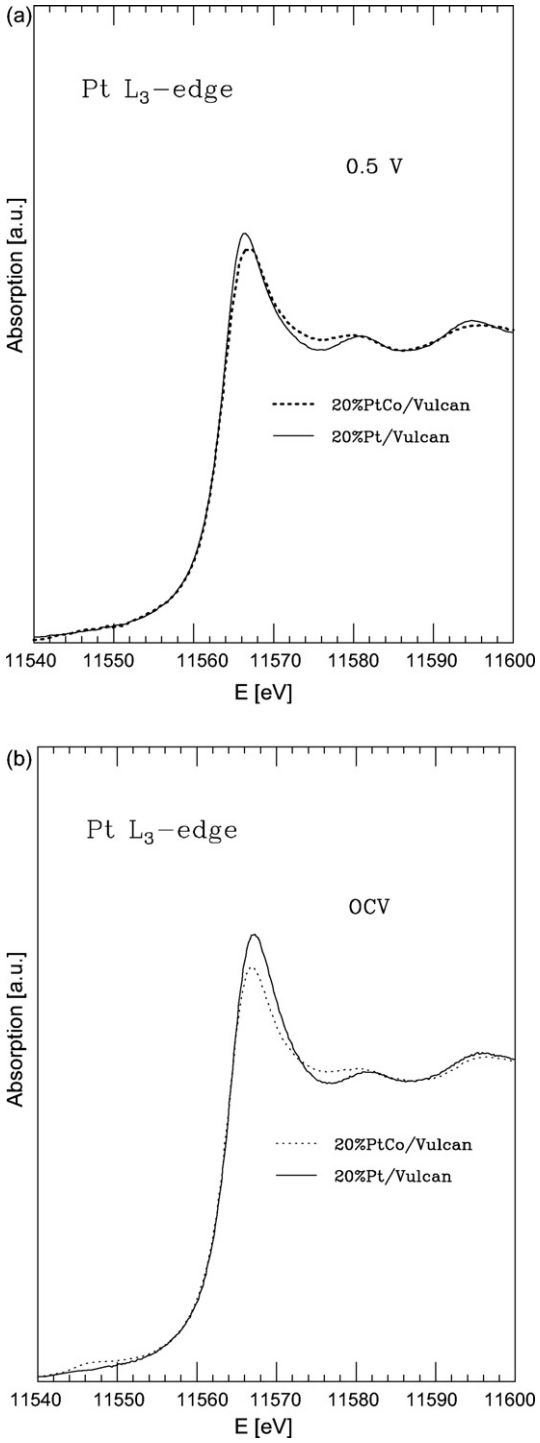

Fig. 5. Comparison of Pt L_3-edge XANES spectra collected in situ at RT (after pre-edge background substraction) of carbon supported 20% Pt–Co (1:1) and 20% Pt electrocatalysts at: (a) 0.5 V; (b) OCV (about 1.0 V).

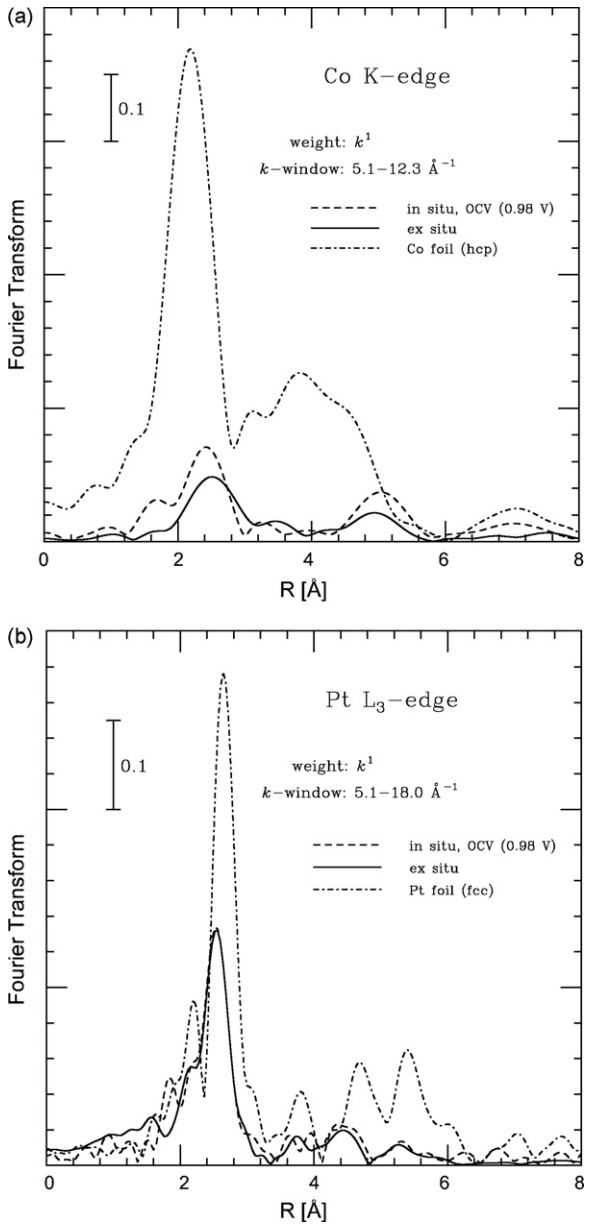

Fig. 6. Fourier transforms of EXAFS spectra of Pt–Co electrocatalyst collected in situ in comparison with spectra of the reference ex situ measurements and foil data: (a) at Co K-edge; (b) at Pt L_3-edge.

- the closer-shell average bond lengths obtained are $R_{Pt–Pt} = 2.721 \pm 0.005$ Å, $R_{Pt–Co} = 2.720 \pm 0.010$ Å and $R_{Co–Co} = 2.700 \pm 0.010$ Å, fully consistent with XRD result;
- in the initial state of the catalyst (ex situ measurements), some contribution of Pt–O configuration has been detected (see the peak at about 1.6 Å in Fig. 6b). The same feature disappears upon exposure of the electrode to the fuel (cf. ex situ and OCV in situ FT);
- after fuel exposure, the observed slight change in the cobalt local structure seems to indicate an increase in order of the structure, probably connected with oxidation;
- in the other in situ measurements, performed at different potential, no tendency to significant difference in the structural values (bond distances and coordination numbers) has been noted.

The results described so far are only preliminary and demonstrate the feasibility of a more detailed analysis of the EXAFS signals. As an example, ongoing data-analysis should permit the accurate determination of the Co atoms positions and clarify the possible occurrence of atomic segregation. Moreover, the effects produced by aging on the catalyst structure will also be examinated.

4. Conclusions

In the present contribution, the preliminary results of in situ fuel cell Co K-edge and Pt L_3-edge XAFS experiments have been presented. The measurements were performed on 20% Pt–Co (1:1) supported on Vulcan (E-TEK) as cathode electrocatalyst (with relatively low metals loading), during fuel cell operation at RT and various potentials.

The results show that:

- the electrochemical cell, as modified for XAS in situ measurements, permits the acquisition of high quality spectra at both the Co K-edge and Pt L_3-edge, which can be processed using advanced data-analysis methods;
- the preliminary analysis performed so far in both XANES and EXAFS regions permits to conclude that, in the nanostructured of (1:1) Pt–Co carbon supported alloy examined, the Pt average local geometric and electronic structure is very similar to that of bulk crystalline platinum and that reversely, the structure of Co is very disordered;
- changes in both geometric and electronic structure are observed upon the fuel exposure, showing Co oxidation and Pt reduction;
- potential-dependent changes are more pronounced in cobalt electronic structure than in platinum one.

Detailed analysis of the data, including ageing effect, is necessary and, at present is underway and it will be the subject of a later communication.

Acknowledgements

We gratefully acknowledge the support of the Synchrotron Light Laboratory ELETTRA in providing synchrotron radiation facilities for the 2006570 experiment carried out at XASF 11.1 Station. Invaluable help from M. Minicucci, L. Olivi and M. Centazzo during measurements are also acknowledged.

This research has been carried out within the NUME Project "Development of composite proton membranes and of innovative electrode configurations for polymer electrolyte fuel cells"(MIUR, FISR 2003).

References

[1] J. McBreen, S. Mukerjee, J. Electrochem. Soc. 142 (1995) 3399–3404.
[2] S. Mukerjee, S. Srinivasan, M.P. Soriaga, J. McBreen, J. Phys. Chem. A 99 (1995) 4577–4589.

[3] E. Antolini, J.R.C. Salgado, E.R. Gonzalez, J. Power Sources 160 (2006) 957–968.
[4] Q. Huang, H. Yang, Y. Tang, T. Lu, D.L. Akins, Electrochem. Commun. 8 (2006) 1220–1224.
[5] M. Min, J. Cho, K. Cho, H. Kim, Electrochim. Acta 45 (2000) 4211–4217.
[6] S.S. Arico, A.K. Shukla, H. Kim, S. Park, M. Min, V. Antoniucci, Appl. Surf. Sci. 172 (2001) 33–40.
[7] T. Toda, H. Igarashi, M. Watanabe, J. Electroanal. Chem. 460 (1999) 258–262.
[8] A.K. Shukla, M. Neergat, P. Bera, V. Jayaram, M.S. Hedge, J. Electroanal. Chem. 504 (2001) 111–119.
[9] F.H.B. Lima, M.J. Giz, E.A. Ticianelli, J. Braz. Chem. Soc. 16 (2005) 328–336.
[10] P.B. Balbuena, D. Altomare, L. Agapito, J.M. Seminario, J. Phys. Chem. B 107 (2003) 13671–13680.
[11] J.M. Seminario, L.A. Agapito, L. Yan, P.B. Balbuena, Chem. Phys. Lett. 410 (2005) 275–281.
[12] L. Guczi, D. Bazin, I. Kovács, L. Borkó, Z. Schay, J. Lynch, P. Parent, C. Lafon, G. Stefler, Zs. Koppány, I. Sajó, Top. Catal. 20 (2002) 129–139.
[13] U.A. Paulus, A. Wokaun, G.G. Scherer, T.J. Schmidt, V. Stamenkovic, V. Radmilovic, N.M. Markovic, P.N. Ross, J. Phys. Chem. B 106 (2002) 4181–4191.
[14] J.R.C. Salgado, E. Antolini, E.R. Gonzalez, J. Power Sources 138 (2004) 56–60.
[15] E. Antolini, J.R.C. Salgado, M.J. Giz, E.R. Gonzalez, Int. J. Hydrogen Energy 30 (2005) 1213–1220.
[16] J.R.C. Salgado, E. Antolini, E.R. Gonzalez, Appl. Catal. B: Environ. 57 (2005) 283–290.
[17] P. Yu, M. Pemberton, P. Plasse, J. Power Sources 144 (2005) 11–20.
[18] F.H.B. Lima, W.H. Lizcano-Valbuena, E. Teixeira-Neto, F.C. Nart, E.R. Gonzalez, E.A. Ticianelli, Electrochim. Acta 52 (2006) 385–393.
[19] A.E. Russell, A. Rose, Chem. Rev. 104 (2004) 4613–4635.
[20] S. Maniquet, R.J. Mathew, A.E. Russell, J. Phys. Chem. B 104 (2000) 1998–2004.
[21] J. McBreen, W.E. O'Grady, K.J. Pandya, P.W. Hoffman, D.E. Sayers, Langmuir 3 (1987) 428–433.
[22] M.E. Herron, S.E. Doyle, S. Pizzini, K.J. Roberts, J. Robinson, G. Hards, F.C. Walsh, J. Electroanal. Chem. 324 (1992) 243–258.
[23] R. Viswanathan, G. Hou, R. Liu, S.R. Bare, F. Modica, G. Mickelson, C.U. Segre, N. Leyarovska, E.S. Smotkin, J. Phys. Chem. B 106 (2002) 3458–3465.
[24] C. Roth, N. Martz, T. Buhrmester, J. Sherer, H. Fuess, Phys. Chem. Chem. Phys. 4 (2002) 3555–3557.
[25] R.J.K. Wiltshire, C.R. King, A. Rose, P.P. Wells, M.P. Hogarth, D. Thompsett, A.E. Russell, Electrochim. Acta 50 (2005) 5208–5217.
[26] E. Principi, A. Di Cicco, A. Witkowska, R. Marassi, J. Synchr. Rad. 14 (3) (2007) 276–281.
[27] A. Witkowska, A. Di Cicco, E. Principi, Phys. Rev. B,. 76 (2007) 104110.
[28] C. Leroux, M.C. Cadeville, V. Pierron-Bohnes, G. Inden, F. Hinz, J. Phys. Met. Phys. 18 (1988) 2033–2051.
[29] N. Travitsky, T. Ripenbein, D. Golodnitsky, Y. Rosenberg, L. Burshtein, E. Peled, J. Power Sources 161 (2006) 782–789.
[30] J. Langford, A. Wilson, J. Appl. Cryst. 11 (1978) 102–113.
[31] R.W.G. Wyckoff, in: Crystal Structures, vol. 1, 2nd ed., John Wiley & Sons, New York-London-Sydney, 1963.
[32] A. Filipponi, A. Di Cicco, C.R. Natoli, Phys. Rev. B 52 (1995) 15122–15134.
[33] A. Filipponi, A. Di Cicco, Phys. Rev. B 52 (1995) 15135–15149.
[34] E.K. Hlil, R. Baudoing-Savois, B. Moraweck, A.J. Renouprez, J. Phys. Chem. 100 (1996) 3102–3107.
[35] A. Kootte, C. Haas, R.A. de Groot, J. Phys. CM 3 (1991) 1133–1152.